Volume 14 | Number 39 | 21 October 2018 | Pages 7937–8074

Soft Matter

rsc.li/soft-matter-journal

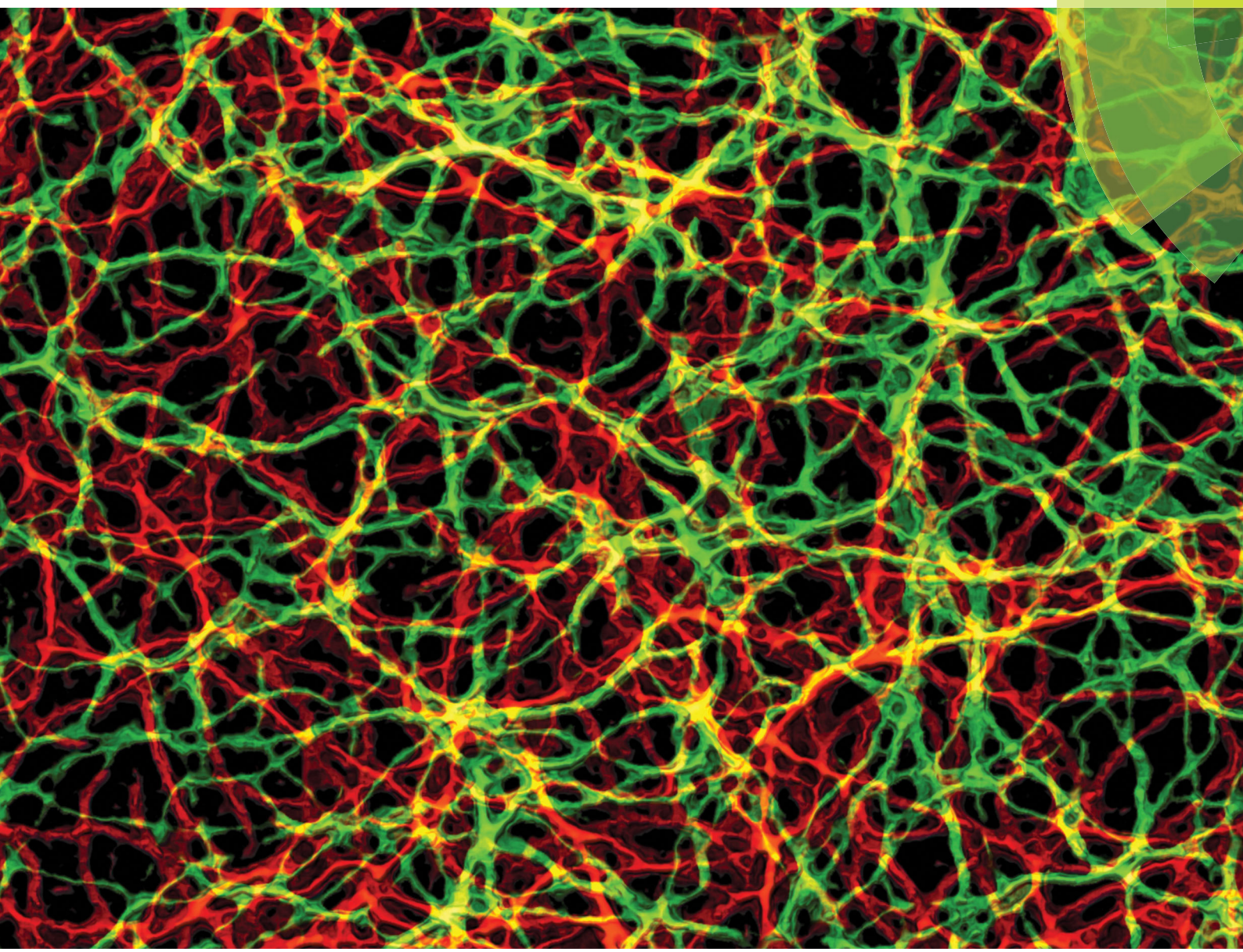

ISSN 1744-6848

ROYAL SOCIETY OF CHEMISTRY

PAPER
Jörg Schnauß *et al.*
Glassy dynamics in composite biopolymer networks

Soft Matter

PAPER

View Article Online
View Journal | View Issue

Cite this: *Soft Matter*, 2018, **14**, 7970

Glassy dynamics in composite biopolymer networks†

Tom Golde,[a] Constantin Huster,[b] Martin Glaser,[ac] Tina Händler,[ac] Harald Herrmann,[de] Josef A. Käs[a] and Jörg Schnauß *[ac]

Received 23rd May 2018,
Accepted 31st July 2018

DOI: 10.1039/c8sm01061g

rsc.li/soft-matter-journal

The cytoskeleton is a highly interconnected meshwork of strongly coupled subsystems providing mechanical stability as well as dynamic functions to cells. To elucidate the underlying biophysical principles, it is central to investigate not only one distinct functional subsystem but rather their interplay as composite biopolymeric structures. Two of the key cytoskeletal elements are actin and vimentin filaments. Here, we show that composite networks reconstituted from actin and vimentin can be described by a superposition of two non-interacting scaffolds. Arising effects are demonstrated in a scale-spanning frame connecting single filament dynamics to macro-rheological network properties. The acquired results of the linear and non-linear bulk mechanics can be captured within an inelastic glassy wormlike chain model. In contrast to previous studies, we find no emergent effects in these composite networks. Thus, our study paves the way to predict the mechanics of the cytoskeleton based on the properties of its single structural components.

Introduction

The cytoskeleton fulfills numerous functions such as determining the cell shape, providing mechanical stability, enabling cell movement and cell division, connecting cells in tissues and influencing signaling within cells.[1,2] It is mainly comprised of three major types of biopolymers: actin filaments (F-actin), microtubules (MT) and intermediate filaments (IFs), which play different roles in the various cell functions. F-actin, for instance, is present in all eukaryotic cells and its contribution to cell mechanics and dynamics has been investigated in great detail.[1] MT are likewise involved in very dynamic processes such as inner-cellular transport and cell division while also supporting the mechanical integrity of the cytoskeleton.[1] In contrast to these two cytoskeletal components, the properties of IF gained less scientific attention and some of their functions remain enigmatic. However, various of their tasks have already been identified and it has been shown that keratin IF determine the stiffness of keratinocytes to a greater extent than the actin cortex.[3,4] In contrast, vimentin IF contribute little to cortical stiffness but play a critical role for intracellular mechanics to protect cells against large stresses and can effectively act as a "cellular safety belt".[5–8] Besides their mechanical properties, vimentin IFs replace keratin IFs during the epithelial to mesenchymal transition (EMT) and are effectively used as a marker for mesenchymal stem cells.[9] Since EMT is central to pathological changes such as fibrosis and cancer metastasis,[9,10] which are inherently linked to changes in cell mechanics,[1] the question arises if the expression of vimentin during the EMT can be justified with physical arguments. The interplay with the actin cytoskeleton is of special interest since it is also altered during EMT. However, physical properties of these biopolymers have been mainly investigated by measuring and comparing reconstituted networks consisting of only one of these components.[11,12] These studies inherently lack the ability to predict the properties of composite networks and only during the past years the focus has been shifted towards a more unifying approach of understanding the interactions of the cytoskeletal subsystems.[13] Composite networks of F-actin and MT, for instance, have been shown experimentally and theoretically to drastically change the non-linear behavior when few MT are embedded in actin networks.[14,15]

Although the interplay within composite F-actin and vimentin IF networks is of crucial biological importance, there are only few rudimentary *in vitro* studies with contradictory results. These studies report both stronger and weaker mechanical properties for the composite networks compared to their pure counterparts depending on the protein density,[16] cross-linker density,[17] and involved phospholipids.[18] Interestingly, these results imply

[a] *Peter Debye Institute for Soft Matter Physics, University of Leipzig, 04103 Leipzig, Germany. E-mail: joerg.schnauss@uni-leipzig.de*
[b] *Institute for Theoretical Physics, University of Leipzig, 04103 Leipzig, Germany*
[c] *Fraunhofer Institute for Cell Therapy and Immunology, 04103 Leipzig, Germany*
[d] *Molecular Genetics, German Cancer Research Center, 69120 Heidelberg, Germany*
[e] *Department of Neuropathology, University Hospital Erlangen, 91054, Erlangen, Germany*

† Electronic supplementary information (ESI) available. See DOI: 10.1039/c8sm01061g

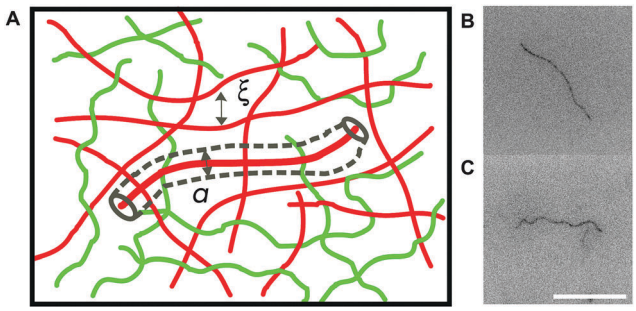

Fig. 1 Tube width and mesh size in composite networks. (A) Sketch of a semidilute, semiflexible polymer network composed of two different biopolymers (red and green). Each filament is confined by the surrounding filaments to a tube-like region with diameter *a*, the so-called tube width. The mesh size ξ is the average space between neighboring filaments. Both quantities are closely connected *via* the persistence length and the contour length of each filament (see eqn (2)). The fluorescence microscopy pictures display (B) an actin filament stabilized with phalloidin and (C) a vimentin filament, which are surrounded by the same composite network of non-labeled actin and vimentin filaments. Note the different contour of the vimentin filament compared to the actin filament demonstrating its higher flexibility. The scale bar is 20 μm.

emergent behaviors when mixing actin and vimentin, which would impose major difficulties for cells to systematically adapt their mechanical properties when needed. However, the previous studies do not take fundamental geometrical parameters such as the networks' mesh size ξ into account, which directly impacts mechanical properties. This hampers the interpretation of these results since the same monomer concentration of actin and vimentin yields networks of different mesh sizes. With respect to the impact on cell mechanics, actin–vimentin interactions might be a reason for increased vimentin expression (instead of keratin) during EMT.

These previous studies also lack consistent and quantitative theoretical models explaining the presented results, which would have inevitably taken the central parameter mesh size into account. The mesh size expresses the average space between neighboring filaments and only depends on the monomer concentration (Fig. 1A), which shows a different scaling for F-actin and vimentin IF. ξ is therefore the main determinant of the concentration scaling in various network models such as the affine deformation model,[19] the tube model,[20] and simple unit cell models.[21] Here, we now compare composite networks with a constant mesh size instead of a constant monomer concentration. Any differences in network properties are consequently only caused by the different properties of actin and vimentin filaments respectively, and not simply by a different spacing.

Experimental

Protein preparation

G-actin was prepared from rabbit muscle and stored at −80 °C in G-Buffer (2 mM sodium phosphate buffer pH 7.5, 0.2 mM ATP, 0.1 mM $CaCl_2$, 1 mM DTT, 0.01% NaN_3) as described previously.[22] For the experiments, small volumes of monomeric actin where thawed and kept on ice until used. Fluorescently labeled actin was prepared by polymerizing G-actin at 5 μM in a 1 : 1 ratio with phalloidin–tetramethylrhodamine B isothiocyanate (phalloidin–TRITC – Sigma-Aldrich Co.). Samples where polymerized by adding 1/10 volume fraction of 10 times concentrated F-buffer (20 mM sodium phosphate buffer pH 7.5, 1 M KCl, 10 mM $MgCl_2$, 2 mM ATP, 10 mM DTT).

Human vimentin was expressed recombinantly in *E. coli* and purified from inclusion bodies as described previously.[23] For visualization, vimentin was fluorescently labeled with Alexa Fluor 488 C5 Maleimide (Thermo Fisher Scientific) according to the method described by Winheim *et al.*[24] with the minor change that the excess dye was removed by elution over PD-10 Desalting Columns (GE Healthcare). The purified vimentin was dialyzed stepwise from 8 M urea against a 2 mM sodium phosphate buffer at pH 7.5 and stored on ice before polymerization into filaments.[25] For experiments requiring fluorescently labeled vimentin about 10% of the monomers were labeled. The polymerization was initiated with the identical conditions as for actin.

Composite networks were prepared by mixing monomeric actin and vimentin, which were subsequently polymerized by adding 1/10 volume fraction of 10 times concentrated F-buffer. This co-polymerization enabled the formation of the fully mixed, composite networks with interwoven filaments (Fig. S1 in the ESI†).

Single filament observation

Samples for single filament observations were prepared and analyzed similarly to the method described by Schuldt *et al.*,[26] which will be shortly summarized here. Both fluorescently labeled actin and vimentin filaments were polymerized at 0.2 g l^{-1} for one hour at room temperature. Labeled filaments were diluted and gently mixed with unlabeled monomers to a molar ratio between 1 : 2000 and 1 : 20 000 and polymerized for one hour at 37 °C. (±)-6-Hydroxy-2,5,7,8-tetramethylchromane-2-carboxylic acid (Trolox – Sigma-Aldrich Co.) was added to a final concentration of 2 mM as an anti-photobleaching agent due to its radical scavenging and antioxidant activities. The mixtures of labeled filaments embedded in an unlabeled network were placed between two glass slides, as described by Golde *et al.*[27] These final samples were kept at room temperature for one hour prior to observation. Specimen with pure vimentin were polymerized directly in the sample chamber for two hours at room temperature.

Images of the embedded tracer filaments were recorded *via* an epifluorescence microscope (Leica DM-IRB, 100× oil objective, NA 1.35) equipped with a CCD camera (Andor iXon DV887). At least 10 filaments were captured in each sample with a frame rate of 10 Hz for 10 s. These filaments were chosen to be well away from the glass surface and had to lie within the focal plane to enable 2D tracking. In samples containing both labeled actin and vimentin filaments, the polymers could be easily distinguished by using different filter cubes for TRITC–phalloidin (red) and Alexa 488 (green). Filament tracking was performed with the freely available ImageJ plugin JFilament (http://imagej.nih.gov/ij/).

This tracking data was used to determine tube widths and mesh sizes. All images of a single filament where summed up and a mean tube backbone was tracked from this overlay. Perpendicular

profile lines of the mean tube backbone were drawn to determine intersection points with all individual filament tracks. After estimating a kernel density at each intersection point and fitting by a Gaussian, the tube width was defined as twice the standard deviation of the Gaussian. The final tube width of a filament is the mean of all intersection points in the center region of the tube.

The same data was used to obtain the MSD of single filaments presented in Fig. 4. Here, the filament center was defined as the point at the backbone with an equal distance to both ends. Its movement was analyzed as a projection on the tangent vector of the tube backbone at the corresponding position. Our definition of the filament center is susceptible to fluctuations of the contour length caused by tracking errors and filament ends moving out of focus. Thus, we compared the MSD of the filament center to the MSD of the contour length over time divided by 4. Filaments with a non-constant MSD of the contour length were excluded from analysis. For filaments where both the MSD of the contour length and the MSD of the filament center are constant and comparably small, the latter is only an upper bound of the actual filament movement.

Shear rheology

Shear rheology measurements were performed with a strain controlled ARES rheometer (TA Instruments, USA) and a plate–plate geometry with a diameter of 40 mm and a gap width of 140 μm. All components were mixed on ice and polymerized directly between the two plates for 2 hours at 25 °C. F-Buffer with the same conditions as in the sample was added to the sides of the plates to prevent artifacts from interfacial elasticity.[28,29] The sample chamber was sealed with a cap equipped with wet sponges to prevent evaporation. Filament assembly was monitored with a dynamic time sweep by a short measurement every 60 s at a frequency of 1 Hz and a strain of 5%. Samples that appeared to be out of equilibrium at the end of the time sweep were excluded from analysis. The linear regime was measured with a dynamic frequency sweep with a strain of 5% and 20 points per decade.

The non-linear regime was tested with a transient step rate measurement and strain rates of 0.025 s^{-1}, 0.1 s^{-1} and 0.25 s^{-1}. The differential shear modulus K was determined from the resulting stress–strain curves with a self written MatLab script. After smoothing the data with a spline fit, K was calculated as the gradient of the stress divided by the strain step width. The linear value K_{lin} was defined at the first non-negative stress value. Negative stress values for small strains are simply a result of measurement limitations as well as the spline fit and do not resemble any physical meaning. K_{lin} was verified to scale linearly with the linear elastic plateau modulus $G_0 = G'(f = 1\ \text{Hz})$ (Fig. S2F of ESI†).

Results and discussion

Mesh size

The mesh size of a semiflexible polymer network can be estimated by assuming a simple cubic network of rigid rods with the mass per length m_L and the protein concentration c:

$$\xi = \sqrt{\frac{3m_L}{c}}. \quad (1)$$

With $m_L = 2.66 \times 10^{-11}$ g m^{-1} for F-actin[30] and $m_L = 5.48 \times 10^{-11}$ g m^{-1} for vimentin filaments,[31,32] both actin and vimentin filament networks should have the same $\xi = 0.4$ μm for $c_{actin} = 0.5$ g l^{-1} and $c_{vimentin} = 1.0$ g l^{-1}. Using these values as boundary conditions, we can chose actin–vimentin mixtures with the same total polymer length per unit volume and consequently the same theoretical mesh size.

We determined the mesh size in our networks directly by observing embedded fluorescent tracer filaments as described previously by Schuldt *et al.*[26] (Fig. 1). Measuring the tube width a of these filaments with persistence length l_P, we calculated the mesh size ξ of our networks with the relation

$$a \approx 0.31\frac{\xi^{6/5}}{l_P^{1/5}} + 0.56\frac{\xi^2}{L}, \quad (2)$$

where L is the contour length of the filament. The prefactors in eqn (2) were determined in computer simulations and the obtained mesh size represents only an upper limit of the actual mesh size in the network.[33] With this method, ξ can be obtained for each sample with a typical standard deviation between 0.1 μm and 0.4 μm due to the filament-to-filament variation of the tube width within one sample. For pure F-actin as well as vimentin filament networks the concentration scaling of ξ is in good agreement with a power law exponent of $\alpha = -0.5$ as predicted by the tube model[34] (Fig. S3 of ESI†).

The scaling of the persistence length in eqn (2) was tested by employing fractions of both populations fluorescently labeled (vimentin filaments with $l_P = 2$ μm[35,36] and phalloidin stabilized F-actin with $l_P = 17$ μm[20]) and embedded in the same composite network (Fig. 2A). In these networks vimentin filaments have a larger tube width than F-actin due to their higher flexibility (Fig. S3 of ESI†). Comparing the mesh sizes obtained from all actin and vimentin filaments in each sample, the difference of the mean values between actin and vimentin is smaller than the sample to sample variation (Fig. 2A). Thus, both labeled actin and vimentin filaments can be used independently for determining ξ despite their different persistence length. Calculating the weighted mean from all actin, vimentin, and composite samples we obtained a mesh size of $\xi = 1.16 \pm 0.24$ μm (Fig. 2B).

Alternatively, the mesh size can be obtained by tracking embedded particles of different sizes. For actin, it has been shown that this technique leads to the same scaling of ξ with protein concentration as the filament tracking.[37] The thermal motion of tracer particles with a radius similar to the mesh size is very sensitive to the ratio of both values.[38,39] The actual value for ξ, however, can only be roughly approximated, as well. For vimentin, ξ was determined as an upper bound of the real mesh size with a value between 1.2 μm and 1.5 μm at a concentration of 1 g l^{-1}.[40] Schopferer *et al.* calculated the size mesh from the elastic plateau modulus obtained with bulk rheology by assuming a simple network of flexible chains.[41] This approach completely neglects the influence of the persistence length and attractive interactions between vimentin filaments. The obtained value of $\xi = 0.175$ μm can at most be regarded as a lower bound. Considering the large variation of the mesh size in the literature,

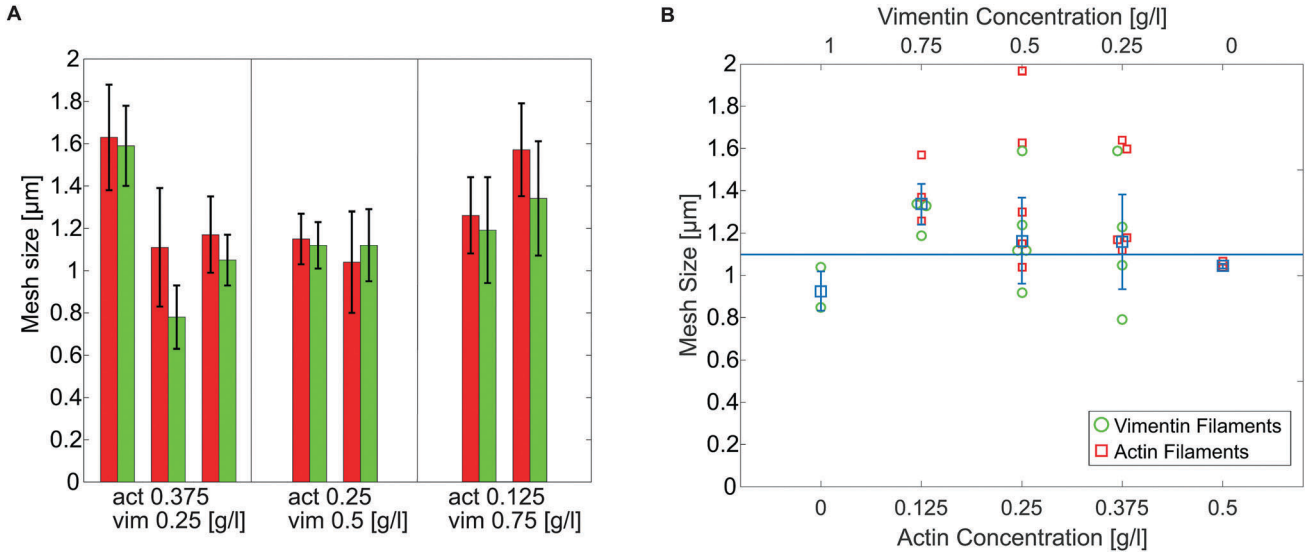

Fig. 2 (A) Mesh sizes of composite networks at different actin/vimentin ratios obtained by measuring the tube width of embedded actin (red) and vimentin (green) filaments. Each bar is the mean value of approximately 10 filaments. Adjacent green and red bars belong to the same sample illustrating that the network architecture can be determined independent of the filament type. Differences between the actin and vimentin mesh size are in average smaller than the sample to sample variation. Error bars represent the standard deviation of the mean value. (B) Each data point is the weighted mean of all actin (red squares) or vimentin (green circles) filaments within one sample containing approximately 10 filaments each. Blue squares display the weighted means of the presented samples and error bars represent the standard deviation of the mean. The blue line illustrates the mean value of all analyzed samples showing that the different mixing ratios result in same network mesh size.

we conclude that using tracer filaments is a very suitable method to compare ξ quantitatively in different semiflexible biopolymer networks.

Superposition in the linear deformation regime

With the microscopic properties we are able to establish composite networks with comparable architectures. This aspect is essential to systematically investigate their macro-rheological behavior since they feature the same mesh size and differ only in the relative composition of actin and vimentin filaments. Using bulk shear rheology, we measured the complex shear modulus $G^*(f) = G'(f) + iG''(f)$ and found the highest mean elastic modulus $G_0 = G'(f = 1\ \text{Hz})$ of 2.6 Pa for pure vimentin IF networks. This value gradually decreases for composite networks with less vimentin content until reaching pure F-actin networks with $G_0 = 1.5$ Pa (Fig. 3A and Fig. S5 of ESI†). Following the same

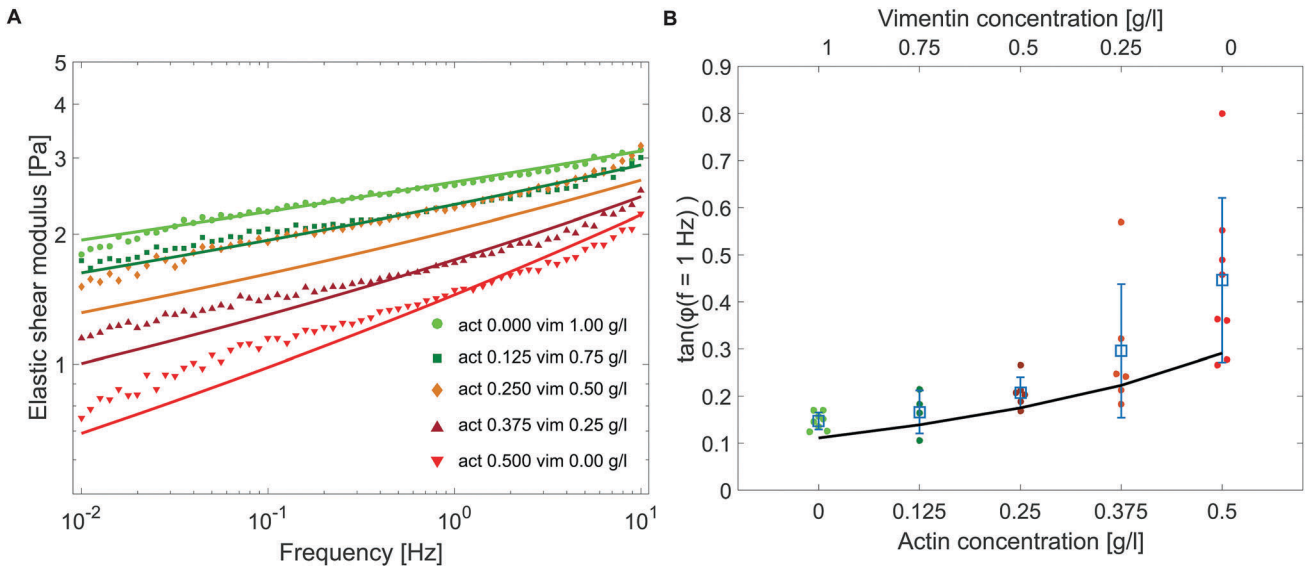

Fig. 3 (A) The dashed lines represent the mean values of measured $G'(f)$ while the continuous lines are the according fits from the GWLC illustrating the gradual decrease of $G'(f)$ with decreasing vimentin/increasing actin content. (B) Mean values of the loss factor $\tan(\phi)$ at $f = 1$ Hz with standard deviations. The dots represent the results of single measurements and the continuous line is the loss factor from the fit using the GLWC.

direction, the loss factor $\tan(\phi) = G''/G'$ increases from very elastic vimentin filament networks with $\tan(\phi(f = 1\ \text{Hz})) = 0.15$ to less elastic F-actin networks with $\tan(\phi(f = 1\ \text{Hz})) = 0.45$ (Fig. 3B). Composite networks of actin and vimentin filaments reveal intermediate properties between the extremes.

These findings are in contrast to the results by Esue *et al.* presenting emergent properties of composite networks with a higher stiffness than the pure counterparts.[16] In this study, however, the monomer concentration was held constant leading to varying mesh sizes, *i.e.* different network architectures, which renders a quantitative comparison non-trivial.

Our data can be explained with the help of the glassy wormlike chain (GWLC) model proposed by Kroy and Glaser.[42] The basic idea of this simple phenomenological model is an exponential stretching of the filament mode relaxation times $\tau_\lambda > \tau_\Lambda$ of all eigenmodes of (half) wavelength λ longer than a characteristic interaction length Λ, by multiplying a factor $\exp(\varepsilon N)$. Λ determines the number $N \equiv \lambda/\Lambda - 1$ of interactions per wavelength λ and corresponds to the entanglement length.[43] The stretching parameter ε can be understood as the characteristic strength of the free energy barriers in units of k_BT or, in simple words, as a form of kinetic stickiness of the polymers. A more detailed description of the GWLC is presented in ESI text (ESI†).

The analysis was performed using self-written Mathematica (Wolfram Research) scripts. The fit of the linear rheology data of the pure actin and the pure vimentin networks were obtained by simultaneously fitting the storage modulus $G'(f)$ and the loss factor $\tan(\phi(f))$ to the mean curves of our measured data with

$$G^*(\omega) = \frac{\Lambda}{5\xi^2\chi(\omega)}, \tag{3}$$

where $\omega = 2\pi f$ and $\chi(\omega)$ is the micro-rheological linear response function of the GWLC to a point force at its ends (see ESI text for details, ESI†). To minimize the number of fit parameters to merely two, namely the interaction length Λ and the stretching parameter ε, we fixed all other parameters to experimental or reference values, respectively. For the contour lengths we used the median of all fluorescently labeled filaments (Fig. S4 of ESI†). This method neglects very short filaments and leads to longer values than typically obtained from electron microscopy measurements. It is still a reasonable estimate for our model as longer filaments also contribute to a greater extent to the network properties. The mesh size for pure networks was fixed to 1 μm and the friction $\zeta_\perp$ was set to a typical value for water. For l_p we used 2 μm for vimentin[36] and 10 μm for actin.[20] In addition, we checked that including a non-zero pretension into the description did not lead to qualitative different results. The used parameters are summarized in Table S1 (ESI†).

The fit quality is very good for both vimentin ($R^2 = 0.977$) and actin ($R^2 = 0.979$) samples. However, there is an apparent deviation of the fit with the frequency dependence of the elastic modulus $G'(f)$ and the magnitude of the loss factor $\tan(\phi(f = 1\ \text{Hz}))$ for F-actin. Both quantities cannot be considered independent of each other but are in fact related *via* the Kramers–Kronig relation.[44] For F-actin, the mean shear modulus is not a perfect representation of the network ensemble due to the large sample to sample variation. Thus, there is a stronger deviation between model and data.

We find $\varepsilon = 2.6$ and $\Lambda = 95$ nm for actin while for vimentin $\varepsilon = 25.0$ and $\Lambda = 74$ nm. Different definitions of the fixed parameters, *e.g.* using the mean contour length instead of the median, lead to slightly different values for ε and Λ. The pronounced differences between actin and vimentin are thereby more important than the absolute values. We interpret ε as the contribution from unspecific (binding) interactions between filaments. For vimentin those interactions are more pronounced and arise from inherent hydrophobic interactions[45] as well as divalent ions in the buffer.[46] The non-vanishing ε for actin can be attributed to minor impurities and aging effects that are believed to be the main reason for the batch-to-batch variation in reconstituted F-actin networks.[47]

Interestingly, all composite networks can be described as a superposition of the underlying sub-networks. In this context, we can understand the shear modulus as the product of a micro-rheological shear modulus $g^*(f) = \Lambda/5\chi(f)$ with the dimension of a force and an effective concentration scaling. Thus, the complex shear modulus of composite networks can be written as

$$G^*(f)_{\text{composite}} = \frac{{g_{\text{vimentin}}}^*(f)}{{\xi_{\text{vimentin}}}^2} + \frac{{g_{\text{actin}}}^*(f)}{{\xi_{\text{actin}}}^2}, \tag{4}$$

with $\xi = \xi_0\sqrt{c_0/c}$. Here, ξ_0 and c_0 are the mesh size and protein concentration of the pure networks as boundary conditions and c is the protein concentration within the composite network. With this simple assumption, we can capture the results for both $G'(f)$ and $\tan(\phi)$ as presented in Fig. 3 and Fig. S6 of ESI† by using the previously fitted results for ${g_{\text{vimentin}}}^*$ and ${g_{\text{actin}}}^*$. The small deviations between model and data are again a result of the sample to sample variation affecting the mean shear modulus.

We want to emphasize that the frequency dependency of $G^*(f)$ is more meaningful than the value of the plateau modulus G_0. The simple scaling of G_0 with concentration can be explained with the tube model for actin[48] and with the affine model for vimentin in the presence of $MgCl_2$.[46] However, both models result in a frequency independent plateau of $G'(f)$ in the intermediate frequency regime probed by macro-rheology. In contrast to a plateau, we find a very flat slope of $G'(f)$ for pure vimentin that increases gradually with the actin content. G_0 is consequently not a real plateau modulus but rather a rough estimate of the network stiffness. Additionally, there is recent experimental evidence that the tube model is not able predict the correct scaling of G_0 with persistence length l_P.[26,49] We cannot formulate an alternative persistence length scaling with the GWLC because l_P is not only a simple pre-factor for the linear response function $\chi(\omega)$, but influences the mode relaxation times τ_λ and the interaction length Λ, as well. It is conceivable that filament interactions represented by the stretching parameter ε constitute an important factor for the discrepancies between established models and experimental data.

The superposition of our composite networks is even independent of the model. For example, it is possible to approximate $G'(f)$ of actin and vimentin with a simple power law although the actual functional dependence in the GWLC model is more complicated. This allows to replicate $G'(f)_{\text{composite}}$ with the same concentration scaling used in eqn (4) and demonstrates the robustness of our conclusion that there are no apparent attractive forces between actin and vimentin filaments. In the following paragraphs, we will demonstrate that the superposition GWLC model is even consistent in the non-linear deformation regime and the behavior of single filaments.

Differential shear modulus in the non-linear regime

To verify our interpretations of the results in the linear regime, we also tested for additive effects in the non-linear regime. Thus, we measured the differential shear modulus K as the local derivative of stress σ over strain γ with a $\dot{\gamma}$-protocol as described by Semmrich *et al.*[50] (Fig. 4). For actin, we see weak to no strain-stiffening effects as expected from previously published results.[50] Vimentin, in contrast, has a more pronounced linear regime followed by weak strain-softening before a strong strain-stiffening sets in with significant higher γ and $K_{\max}$ than for actin, which is in agreement with previous studies.[45] Composite networks feature an intermediate behavior without any apparent emergent effects. In fact, most of the single curves have two clearly distinguishable peaks (Fig. S2 and S7 of ESI†) and other peaks in the mean curves presented in Fig. 4 are only an artifact of the averaging process.

The parameters obtained from fitting $G^*(f)$ can be used to qualitatively replicate the measured K-curves in the frame of the GWLC. For this purpose, we use the linear shear-modulus evaluated at a constant frequency

$$|G_\omega^*|(F) = \frac{\Lambda}{5\xi^2|\chi_\omega|(F)}, \tag{5}$$

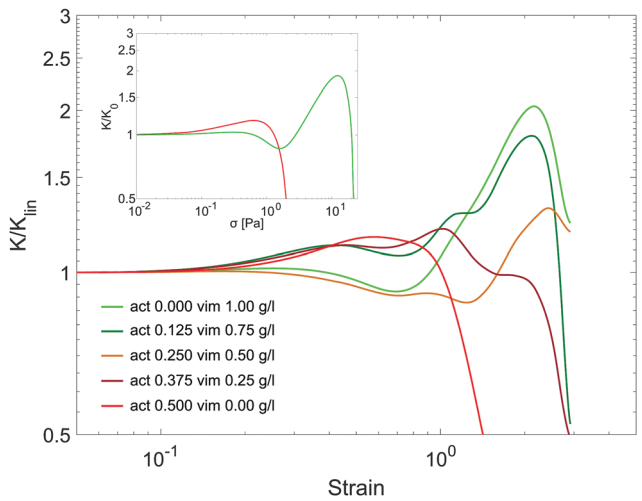

Fig. 4 Stiffening in biopolymer networks. The differential shear modulus K rescaled by its linear value K_{lin} *versus* strain, which was obtained from the mean stress–strain-curves, revealed that composite networks feature the properties of the underlying sub-systems. The inset shows K *versus* stress σ replicated with the GLWC for actin (red) and vimentin (green).

as a function of pre-tension F to model $K(\sigma)$ as proposed by Semmrich *et al.*[50] The macroscopic stress σ is related to F *via* $F = 5\sigma\xi^2$ and ω is fixed to the employed strain rate $\dot{\gamma}$. A linear barrier height reduction in the spirit of the Bell–Evens model[51] is introduced to account for the effect of pre-tension on the stretching parameter:

$$\varepsilon \rightarrow \varepsilon - F\delta/k_{\text{B}}T, \tag{6}$$

where δ should be interpreted as an effective width of a free energy well. In this simple extension, K is a function of stress in contrast to the experimental value that was measured over strain. Nevertheless, we can use δ as the only free parameter to reproduce the observed phenomenology of actin networks qualitatively: an initial phase dominated by stress stiffening related to the non-linear elasticity of semiflexible polymers followed by a stress softening dominated phase, in which force induced fluidization represented by changes of the GWLC relaxation spectrum overcompensates the stress stiffening (Fig. 4 inset).

For vimentin networks, however, the phenomenology is more complicated due to the additional, initial softening regime. A plausible candidate for such a mechanism is the force induced lengthening of vimentin filaments resulting from the slippage of proto-filaments.[52] In contrast to F-actin, vimentin filaments can be stretched more than 3-fold without breaking[8] and there is strong evidence that this mechanism can also be found in vimentin networks.[53] Thus, we focus on modeling the observed phenomenology by extending the GWLC model with the introduction of a force dependent filament length (ESI Text and Fig. S8 for details, ESI†). This model qualitatively reproduces the non-linear behavior of vimentin (Fig. 4 inset).

Other possible softening mechanisms include the occurrence of force induced slip events probably related to occasional disentanglement of some polymers. This can lead to an inelastic deformation that constitutes a softening effect not included in the GWLC.[54,55] There might be mechanisms related to a partial, force induced disentanglement such as an increase in mesh size or changes in the network architecture (*e.g.* shear alignment) that can lead to an additional softening regime, as well. The occurrence of these effects can not be excluded completely. However, there is no straight forward explanation why they should play a role in vimentin but not in F-actin networks.

It may be tempting to use a simple linear combination of K_{actin} and K_{vimentin} for $K_{\text{composite}}$, as demonstrated in the linear regime. Such a superposition cannot be justified due to underlying inherently non-linear mechanisms. We expect that it is possible to model composite networks as two non-interacting networks with different ε. This detailed modeling in the frame of the GWLC, however, is beyond the scope of this work.

Stickiness in single filament observation

In the previous paragraphs we showed that the higher stretching parameter of vimentin compared to actin is the main contribution of the observed differences in both the linear and non-linear regime. In principle, it should be possible to determine ε directly from single filament fluctuations. However, we are not able to measure ε due to a limited range of exposure and observation

times. Another way to investigate the stickiness is the analysis of the mean-squared displacement (MSD) of the filament center parallel to the tube to visualize a retarded reptation for lag times between 0.1 s and 2.5 s (Fig. S9 of ESI†). There exist various theories for the reptation of semiflexible filaments in semi-dilute solutions leading to different predictions about cross-over times and the scaling of the MSD.[34,43,56,57] Thus, we limit our analysis to the value of the MSD in the intermediate time regime between the entanglement time and the rouse time.[57,58] For actin, we typically see this weak power law regime for lag times $\tau \geq 1$ s. For vimentin, we find filaments where the MSD is almost a plateau for all lag times meaning the filament motion is below the noise level of this measurement. Nevertheless, we can use the MSD at the lag time $\tau = 2$ s to analyze the different behavior of actin and vimentin filaments quantitatively, although this approach overestimates the MSD ($\tau = 2$ s) for vimentin (see Experimental for details).

Comparing the MSD ($\tau = 2$ s) in pure actin and vimentin networks we see roughly a linear scaling with the tube width of each filament as predicted by reptation models[56,57] (Fig. 5 inset). Therefore, the MSD has to be rescaled by the tube width to enable a quantitative analysis. Despite the high filament-to-filament variation, the MSD ($\tau = 2$ s)/a of F-actin is significantly larger than for vimentin filaments in both pure and composite networks (Fig. 5 and Fig. S10 of ESI†). There are no significant differences in the filament behavior between different composite networks.

In general, the MSD ($\tau = 2$ s) is expected to increase for more flexible polymers as the main mode of transportation in this time regime arises from the fluctuations of the filaments. In our case, we see the opposite behavior where F-actin has a higher persistence length than vimentin filaments but also a stronger reptation along the tube. This result becomes clear, if we identify the stickiness ε as an effective friction ζ that slows down filament reptation (see also ESI text, ESI†). Thus, we can use the MSD of single filaments to compare the effective filament friction in our samples. This quantitative difference is consequently consistent with the significant higher ε for vimentin.

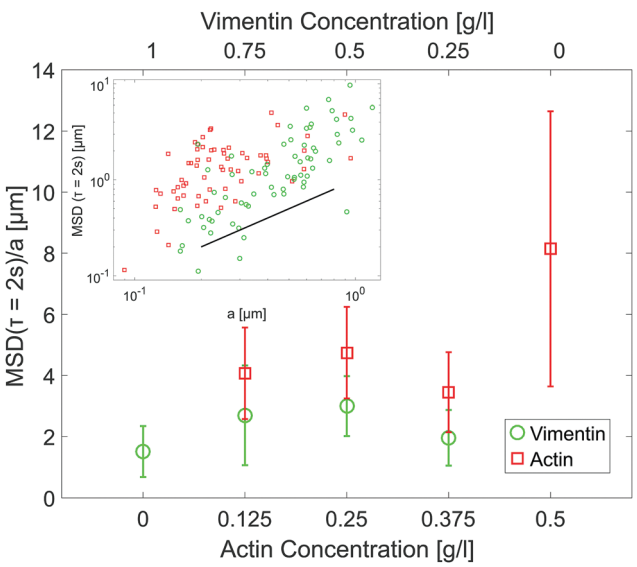

Fig. 5 Single filament tracking. The median MSD of the filament center parallel to the tube at a lag time of 2 s rescaled by tube width a of actin (red squares) and vimentin (green circles) filaments embedded in actin, vimentin, and composite networks. This illustrates the lower motility of vimentin filaments compared to actin filaments. Error bars are the median absolute deviation with $n \geq 9$. The inset shows the MSD ($\tau = 2$ s) *versus* tube width of single actin (red) and vimentin (green) filaments in pure networks. The black line illustrates a linear scaling as a guide to the eye.

Conclusion

In conclusion, by linking single filament behavior directly to macroscopic network properties, we have shown that the mechanical properties of composite networks can be extrapolated from their respective substructures as a superposition in the frame of the GWLC. Stronger inter-filament interactions for vimentin were identified as the main distinction between actin and vimentin filament networks.

The absence of direct actin–vimentin interactions suggests that cells can tune their mechanics by simply changing the molecular content of one or both components. The cytoskeleton is of course more complicated and contains various passive cross-linking proteins as well as motor proteins acting as active cross-linkers. Inherently complex emergent effects between actin and vimentin, as reported in previous studies, would interfere with a precise control of the network behavior through cross-linking mechanisms. Our findings clearly emphasize that sophisticated, concentration-depended feedback mechanisms are unnecessary for cells to adjust their mechanic properties. The next step for understanding interactions between actin and IFs would be composite networks of actin and keratin filaments. Such systems where introduced recently by Deek *et al.*[59] In this study, the architecture of the keratin network is strongly influenced by the presence of F-actin. A rheological characterization of such systems and a comparison with our results could potentially shed new light on the role of vimentin and keratin IFs during EMT.

By incorporating single vimentin filament stretching into the non-linear network behavior, we support the hypothesis that unfolding of IFs provides strength to cells under large deformations[8,52] functioning effectively as a "safety belt".[5] We show that biopolymer networks appear to have a certain degree of interactions even without cross-linking proteins illustrating that they can be neither treated as purely entangled nor cross-linked networks. Thus, the presented study is a step towards bridging the gap between these different theoretical approaches to establish a unifying model that explains biopolymer networks in general by including sticky interactions.

Conflicts of interest

There are no conflicts to declare.

Acknowledgements

We gratefully thank Tatjana Wedig (DKFZ) for electron microscopy and technical assistance with vimentin procedures, and Klaus Kroy for fruitful discussions. Furthermore, we acknowledge funding by the Deutsche Forschungsgemeinschaft for T. H., M. G. (DFG-1116/14-1) and H. H. (HE 1853/11-1) and by the European Research Council (ERC-741350). J. S. acknowledges financial support through the Fraunhofer Attract project 601 683.

Notes and references

1 F. Huber, J. Schnauß, S. Rönicke, P. Rauch, K. Müller, C. Fütterer and J. Käs, *Adv. Phys.*, 2013, **62**, 1–112.
2 H. Herrmann, H. Bär, L. Kreplak, S. V. Strelkov and U. Aebi, *Nat. Rev. Mol. Cell Biol.*, 2007, **8**, 562–573.
3 K. Seltmann, A. W. Fritsch, J. A. Käs and T. M. Magin, *PNAS*, 2013, **110**, 18507–18512.
4 L. Ramms, G. Fabris, R. Windoffer, N. Schwarz, R. Springer, C. Zhou, J. Lazar, S. Stiefel, N. Hersch, U. Schnakenberg, T. M. Magin, R. E. Leube, R. Merkel and B. Hoffmann, *PNAS*, 2013, **110**, 18513–18518.
5 L. Kreplak, H. Bär, J. F. Leterrier, H. Herrmann and U. Aebi, *J. Mol. Biol.*, 2005, **354**, 569–577.
6 M. Guo, A. J. Ehrlicher, S. Mahammad, H. Fabich, M. H. Jensen, J. R. Moore, J. J. Fredberg, R. D. Goldman and D. A. Weitz, *Biophys. J.*, 2013, **105**, 1562–1568.
7 M. G. Mendez, D. Restle and P. A. Janmey, *Biophys. J.*, 2014, **107**, 314–323.
8 J. Block, H. Witt, A. Candelli, E. J. Peterman, G. J. Wuite, A. Janshoff and S. Köster, *Phys. Rev. Lett.*, 2017, **118**, 048101.
9 R. Kalluri and R. A. Weinberg, *J. Clin. Invest.*, 2009, **119**, 1420–1428.
10 D. Hanahan and R. A. Weinberg, *Cell*, 2011, **144**, 646–674.
11 P. A. Janmey, U. Euteneuer, P. Traub and M. Schliwa, *J. Cell Biol.*, 1991, **113**, 155–160.
12 C. Storm, J. J. Pastore, F. C. MacKintosh, T. C. Lubensky and P. A. Janmey, *Nature*, 2005, **435**, 191–194.
13 F. Huber, A. Boire, M. P. López and G. H. Koenderink, *Curr. Opin. Cell Biol.*, 2015, **32**, 39–47.
14 V. Pelletier, N. Gal, P. Fournier and M. L. Kilfoil, *Phys. Rev. Lett.*, 2009, **102**, 188303.
15 Y.-C. Lin, G. H. Koenderink, F. C. MacKintosh and D. A. Weitz, *Soft Matter*, 2011, **7**, 902–906.
16 O. Esue, A. A. Carson, Y. Tseng and D. Wirtz, *J. Biol. Chem.*, 2006, **281**, 30393–30399.
17 M. H. Jensen, E. J. Morris, R. D. Goldman and D. A. Weitz, *BioArchitecture*, 2014, **4**, 138–143.
18 J. V. Shah, L. Z. Wang, P. Traub and P. A. Janmey, *Biol. Bull.*, 1998, **194**, 402–405.
19 F. C. MacKintosh, J. Käs and P. A. Janmey, *Phys. Rev. Lett.*, 1995, **75**, 4425–4428.
20 H. Isambert, P. Venier, A. C. Maggs, A. Fattoum, R. Kassab, D. Pantaloni and M. F. Carlier, *J. Biol. Chem.*, 1995, **270**, 11437–11444.
21 K. Kroy and E. Frey, *Phys. Rev. Lett.*, 1996, **77**, 306–309.
22 B. Gentry, D. Smith and J. Käs, *Phys. Rev. E: Stat., Nonlinear, Soft Matter Phys.*, 2009, **79**, 031916.
23 H. Herrmann, L. Kreplak and U. Aebi, *Methods Cell Biol.*, 2004, **78**, 3–24.
24 S. Winheim, A. R. Hieb, M. Silbermann, E.-M. Surmann, T. Wedig, H. Herrmann, J. Langowski and N. Mücke, *PLoS One*, 2011, **6**, e19202.
25 N. Mücke, T. Wedig, A. Bürer, L. N. Marekov, P. M. Steinert, J. Langowski, U. Aebi and H. Herrmann, *J. Mol. Biol.*, 2004, **340**, 97–114.
26 C. Schuldt, J. Schnauß, T. Händler, M. Glaser, J. Lorenz, T. Golde, J. A. Käs and D. M. Smith, *Phys. Rev. Lett.*, 2016, **117**, 197801.
27 T. Golde, C. Schuldt, J. Schnauß, D. Strehle, M. Glaser and J. Käs, *Phys. Rev. E: Stat., Nonlinear, Soft Matter Phys.*, 2013, **88**, 044601.
28 O. Mueller, H. E. Gaub, M. Baermann and E. Sackmann, *Macromolecules*, 1991, **24**, 3111–3120.
29 S. Yamada, D. Wirtz and P. A. Coulombe, *J. Struct. Biol.*, 2003, **143**, 45–55.
30 A. C. Steven, J. F. Hainfeld, B. L. Trus, J. S. Wall and P. M. Steinert, *J. Biol. Chem.*, 1983, **258**, 8323–8329.
31 H. Herrmann, M. Häner, M. Brettel, S. A. Müller, K. N. Goldie, B. Fedtke, A. Lustig, W. W. Franke and U. Aebi, *J. Mol. Biol.*, 1996, **264**, 933–953.
32 U. Wickert, N. Mücke, T. Wedig, S. A. Müller, U. Aebi and H. Herrmann, *Eur. J. Cell Biol.*, 2005, **84**, 379–391.
33 H. Hinsch, J. Wilhelm and E. Frey, *Eur. Phys. J. E: Soft Matter Biol. Phys.*, 2007, **24**, 35–46.
34 D. C. Morse, *Macromolecules*, 1998, **31**, 7030–7043.
35 N. Mücke, L. Kreplak, R. Kirmse, T. Wedig, H. Herrmann, U. Aebi and J. Langowski, *J. Mol. Biol.*, 2004, **335**, 1241–1250.
36 B. Nöding and S. Köster, *Phys. Rev. Lett.*, 2012, **108**, 088101.
37 C. F. Schmidt, M. Baermann, G. Isenberg and E. Sackmann, *Macromolecules*, 1989, **22**, 3638–3649.
38 M. L. Gardel, M. T. Valentine, J. C. Crocker, A. R. Bausch and D. A. Weitz, *Phys. Rev. Lett.*, 2003, **91**, 158302.
39 I. Y. Wong, M. L. Gardel, D. R. Reichman, E. R. Weeks, M. T. Valentine, A. R. Bausch and D. A. Weitz, *Phys. Rev. Lett.*, 2004, **92**, 178101.
40 S. Köster, Y.-C. Lin, H. Herrmann and D. A. Weitz, *Soft Matter*, 2010, **6**, 1910–1914.
41 M. Schopferer, H. Bär, B. Hochstein, S. Sharma, N. Mücke, H. Herrmann and N. Willenbacher, *J. Mol. Biol.*, 2009, **388**, 133–143.
42 K. Kroy and J. Glaser, *New J. Phys.*, 2007, **9**, 416.
43 A. N. Semenov, *J. Chem. Soc., Faraday Trans.*, 1986, **82**, 317–329.
44 K. Kroy and J. Glaser, *AIP Conf. Proc.*, 2009, **1151**, 52–55.
45 P. Pawelzyk, N. Mücke, H. Herrmann and N. Willenbacher, *PLoS One*, 2014, **9**, e93194.
46 Y.-C. Lin, N. Y. Yao, C. P. Broedersz, H. Herrmann, F. C. MacKintosh and D. A. Weitz, *Phys. Rev. Lett.*, 2010, **104**, 058101.
47 J. Xu, W. H. Schwarz, J. A. Käs, T. P. Stossel, P. A. Janmey and T. D. Pollard, *Biophys. J.*, 1998, **74**, 2731–2740.

48 B. Hinner, M. Tempel, E. Sackmann, K. Kroy and E. Frey, *Phys. Rev. Lett.*, 1998, **81**, 2614–2617.
49 M. Tassieri, *Macromolecules*, 2017, **50**, 5611–5618.
50 C. Semmrich, T. Storz, J. Glaser, R. Merkel, A. R. Bausch and K. Kroy, *PNAS*, 2007, **104**, 20199–20203.
51 G. I. Bell, *et al.*, *Science*, 1978, **200**, 618–627.
52 T. Ackbarow and M. J. Buehler, *J. Mater. Sci.*, 2007, **42**, 8771–8787.
53 I. K. Piechocka, K. A. Jansen, C. P. Broedersz, N. A. Kurniawan, F. C. MacKintosh and G. H. Koenderink, *Soft Matter*, 2016, **12**, 2145–2156.
54 L. Wolff, P. Fernández and K. Kroy, *PLoS One*, 2012, **7**, e40063.
55 M. Gralka and K. Kroy, *Biochim. Biophys. Acta, Mol. Cell Res.*, 2015, **1853**, 3025–3037.
56 M. Doi and S. F. Edwards, *The Theory of Polymer Dynamics*, Clarendon Press, 1988.
57 R. Granek, *J. Phys. II*, 1997, **7**, 1761–1788.
58 T. C. B. McLeish, *Adv. Phys.*, 2002, **51**, 1379–1527.
59 J. Deek, R. Maan, E. Loiseau and A. R. Bausch, *Soft Matter*, 2018, 218–229.